Chapter 10
2D Nanomaterial Photoelectrodes for Photoelectrochemical Degradation of Pollutants and Hydrogen Generation

Pooja Singh, Sweta Sharma, and Pooja Devi

Abstract The development of sustainable solutions for meeting escalating needs, such as clean energy and safe drinking water, is of the utmost importance to the modern world. Hydrogen as a fuel can be worthiest for this purpose, and further generating it from wastewater via green routes, i.e. photo/electrocatalytic splitting, can make it a sustainable solution, overcoming challenges of wastewater treatment simultaneously. In this chapter, we have discussed different materials that can be utilized as photoelectrocatalyst focusing on 2D materials for hydrogen generation from wastewater (textile, pharmaceutical, food industry, etc.). The potential catalytic properties of transition metal dichalcogenides (TMDs), transition metal oxides (TMOs), MXenes, graphene, nitrides, carbides, and their hybrids are discussed for the same. The standard diagnostic parameter for evaluating photoelectrocatalyst is photo response, incident photon to current efficiency, faradaic efficiency, and wastewater treatment in terms of percentage degradation, COD, TOC, etc., are presented and compared for 2D materials. Further, material performance in terms of the band gap, appropriately positioned valence and conduction bands, stability, economics, etc., are also compared for the wastewater systems. Last but not the least, the future outlook of the field is also presented with respect to challenges and research directions to tap this important unused energy source, i.e. wastewater.

Singh and Sharma: Equally contributed.

P. Singh · S. Sharma · P. Devi (✉)
Academy of Scientific and Innovative Research, New Delhi, India
e-mail: poojaiitr@csio.res.in

P. Devi
Materials Science and Sensor Application, Central Scientific Instruments Organisation, Chandigarh 160030, India

N. Kumar et al. (eds.), *Two-Dimensional Materials for Environmental Applications*, Springer Series in Materials Science 332, https://doi.org/10.1007/978-3-031-28756-5_10

10.1 Introduction

To meet the global demand for clean energy and clean water, developing and progressing sustainable solutions and technologies is necessary. In current times, a decarbonized world powered by renewable energy is transitioning, and hydrogen is seen as a clean energy carrier. Thus, hydrogen as a fuel can be worthiest for this and generating it from wastewater in greenways, like the photo/electrocatalytic splitting of water, can also enable wastewater utilization as well as treatment [30]. Hydrogen as a fuel has found tremendous stationery and mobile usage, such as a propellant of non-polluting vehicles, home heating, cooking, chemical transformations, and aviation. Therefore, it is projected that hydrogen will join solar power as the primary energy carrier for a sustainable energy system [4, 27, 90]. Likewise, photocatalytic degradation of organic wastes in a photoelectrochemical (PEC) system is an appealing approach for their complete mineralization. Therefore, a dual system utilizing wastewater as feedstock can address both challenges at the same time [19]. The fundamental photo(electro) catalytic setups of both processes share the same roots, but they are rarely explored concurrently. The most well-known scientific paper that impacted this field's progress was by Fujishima and Honda [1] in 1972, which described photocatalytic water splitting in a PEC cell employing semiconductor photoelectrode.

As a feedstock, wastewater has a rich supply of nutrients like organic compounds, phosphate, nitrogen and minerals, which makes it an enormous source for energy recovery. The current conventional wastewater treatment facilities use a lot of energy, yet many organic/inorganic constituents still remain untreated. Alternatively, wastewater can also be used to generate power, heat, or fuels like hydrogen or methane. Anaerobic digestion, which produces biogas, is one of the most popular and is still the most widely adopted technology for recovering energy from wastewater around the world [5]. This process results in the production of biogas, a gas combination primarily made up of methane and CO_2. Alternatively, hydrogen generation from wastewater is a promising and less explored approach. Some efforts have been made in the direction of biological processes such as fermentation, in particular, photo-fermentation and dark fermentation, for producing biohydrogen [89]. In photo-fermentation, sunlight-powered photosynthetic bacteria convert organic molecules into hydrogen and carbon dioxide. In general, dark fermentation is frequently combined with photo-fermentation; wherein photosynthetic bacteria convert the organic acids produced as a by-product of dark fermentation into hydrogen [56]. Another way of hydrogen production from wastewater is via splitting the water under light (photocatalysis) or electricity (electrocatalysis) or the combination of both (photo (electro)catalysis). On exposure to the light to a photocatalyst system, charge carriers are generated, which in turn can be utilized to drive hydrogen evolution and organic pollutants oxidation in a wastewater environment [70]. The first such system reported by Fujishima and Honda utilized TiO_2 electrodes [1]. Since that time, interest in photocatalysts research has been continuously increasing, leading to the development of plethora of materials in this field. Neverthless, only a few findings

concentrate on producing hydrogen from the wastewater. This may be due to despite of simplicity of the underlying chemistry of water splitting, effective wastewater-to-hydrogen generation is a complicated process due to the involvement of two thermodynamic processes of pollutant mineralization as well as water reduction. It requires specifically designed catalytic electrodes and a significant amount of energy to drive the process. The presence of impurities in the wastewater environment can not only damage the catalysts but also reduce the overall efficiency along with the generation of unwanted by-products. Thus the present chapter is focused on discussing and revieweing 2D materials-based photoelectrodes for a dual-system photo electrochemistry i.e. the simultaneous removal of pollutants from wastewater and hydrogen generation. It also covers the basic understanding of the type of wastewater pollutants, an overview of the PEC fundamentals, a discussion on the class of 2-D materials, and factors affecting their performance in PEC. A critical evaluation of the current state of the art and their limitations in this field is also presented with the projection of future opportunities.

10.2 Wastewater Characteristics

Wastewater is a mixture of liquid or water-carried pollutants removed from households, organizations, and institutions with groundwater, surface water, and stormwater. Wastewater generally includes suspended solids that comprise metals, organic/inorganic substances, disease-causing microorganisms, faecal matter, organic waste, and more [108]. Before entering the treatment facility, wastewater is referred to as influent; after it is released from the facility, it is referred to as effluent. Sludge is the term used to describe the leftover semi-solid waste in the working unit [77]. The following four categories could be employed to categorize it based on the source of contamination:

(A) Domestic wastewater: It is further divided into grey and black garbage. Grey water is the waste from laundry, washrooms, and kitchens, whereas black water is made up of urine and faeces.
(B) Industrial wastewater: Water released by organizations (such as pharma, paper industry, and textile mills) and livestock farming.
(C) Infiltration wastewater: The water is made up of sewerage water that gets contaminated through leaks in joints, gaps, porous roofs, and walls.
(D) Storm wastewater (runoff): It is a combination of sewerage water and flood water from rain [82].

Wastewater can further be categorized according to the physicochemical parameters depending upon the source. Based on these physical and chemical characteristics (as shown in Fig. 10.1), the pre-treatment methods and treatment technologies are selected [9, 81], wherein the water is analyzed for its temperature, pH, color, turbidity, total suspended solids (TSS), and total dissolved solids (TDS), Chemical oxygen demand (COD), biochemical oxygen demand (BOD), total organic carbon

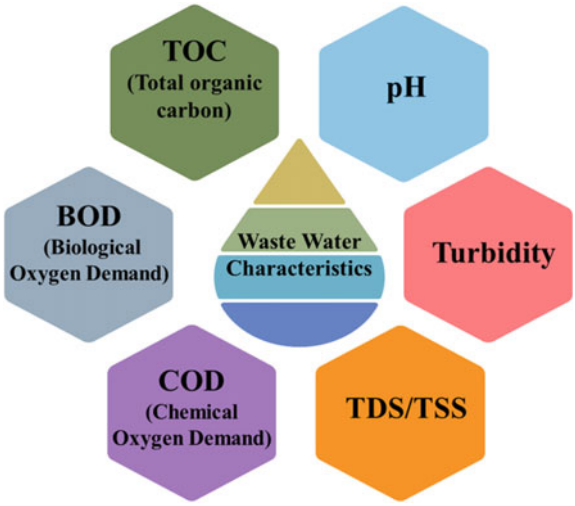

Fig. 10.1 Physical and chemical characteristics of wastewater

(TOC) before and after the treatment. The temperature of influent wastewater mainly ranges from 26.2–35.4 °C [103], while its pH varies from the source of its origin and generally covers a wide range. The broad range of pH of wastewater can change the rate of biochemical reactions in aquatic organisms [85]. The color of the water is also a qualitative factor for the representation of the storage circumstance as well as the presence of a type of organic constituents in the water [85]. Turbidity is another important physical parameter, which is a direct indication of pollutants present in water. The higher amount of turbidity signifies a high concentration of waste or vice-versa [69]. The chemical parameters, i.e. TOC, COD, and BOD, are related to organic constituents present in water [83]. COD determines the amount of oxygen needed for chemically oxidizing organic waste, whereas the overall amount of oxygen microbes required to decompose organic waste in an aerobic environment completely is referred to as BOD. The high level of BOD, COD and TOC signifies a higher level of pollution [61, 64].

10.3 Photoelectrocatalysis Mechanism

A PEC system generally contains three electrodes or a two-electrodes: a counter electrode, reference electrode, and the working electrode (photoanode & photocathode). At least one of the electrodes needs to be a semiconductor capable of absorbing light with higher energy than its bandgap to generate electron and hole pairs. Under external bias, these charge carriers can be separated to perform water reduction to generate hydrogen and pollutant oxidation for mineralization. In general, an externally generated electrical/chemical bias provides the extra voltage required for the reaction i.e. water splitting. While in PEC, the photocatalytic electrodes can collect

solar energy that can help to reduce this energy or completely replace electrical energy based on material characteritsics. A PEC system also has advantages over the standalone photocatalytic system in terms of (i) self and external bias can alleviate the electron–hole recombination and enhance the charge transfer kinetics, (ii) easy separation of hydrogen and oxygen at both the electrodes, (iii) coating of the semiconductor materials onto large area substrates such as conductive and semiconductor substrate, and (iv) increased stability of the catalyst in bound form than the powder catalyst.

In general, based on the type of semiconductor at the working electrode, i.e. n-type-photoanode or p-type-photocathode, the two types of reactions, i.e. hydrogen evolution reaction (HER) and oxygen evolution reaction (OER), occur at the anode and cathode, respectively. In general, the processes in a PEC system are (i) absorption of light and generation of photo charges, (ii) charge separation & charge transfer and (iii) water splitting/redox reaction [71].

(i) **Absorption of light and generation of excitons**: The semiconductor's electrical structure interacts with the electromagnetic wave as light passes through it. This interaction excites certain electrons in the valence band (VB) to enter the conduction band (CB) and create holes in VB. The bandgap of semiconductors is thus the energy difference between the CB and VB. When the photon energy is greater than the semiconductor's band gap, the excited electrons transfer the extra energy to nearby atoms by thermal vibration, stabilizing the CB. Due to their excellent chemical resistance, metal oxide semiconductors have been examined as photoelectrodes; however, due to their large band gap energy, which accounts for 4% of the solar spectrum, their activity is primarily restricted in UV light. Thus efforts are being made to design narrow bandgap semiconductors to overcome this limitation.

(ii) **Charge separation and transfer**: To stop the recombination process, the photo-generated charge carriers at the photoelectrode surface should be separated. Recombination is the principal barrier to charge carriers' transport to the photo electrode's active sites, as it makes it challenging to extract current from charge carriers due to the high recombination degree. The crystal structure and size of the particle of the material affects the rate of recombination. The defects/imperfections can act as a trapping centre, while a high crystalline material exhibits significant photocatalytic activity due to less recombination. In the case of nanomaterials, the recombination is less due to the high surface-to-volume ratio and ease of transport of excitons to the catalyst surface. The transfer of photogenerated charge is further influenced by the morphology of the catalyst on the substrate, it's defect characteristics, and electrolyte composition. For example, charge transfer across the linear transport path can be improved by using 1D nanostructures like nanotubes. Furthermore, an exterior bias or a built-in internal potential can enhance the electron-holes separation and reduce the recombination. The inbuilt potential could be generated by doping metal/non-metal elements, integration of metals onto the semiconductor, and making heterojunctions with materials of different band gaps. Some

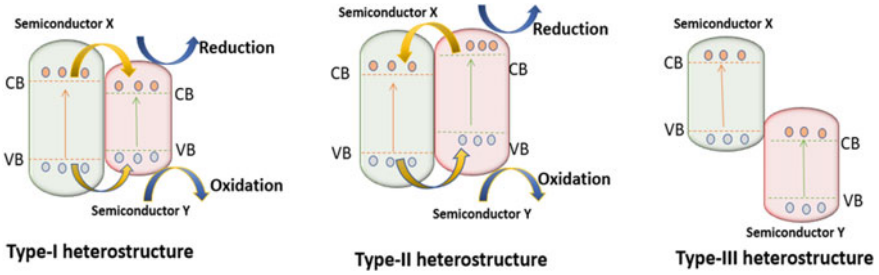

Fig. 10.2 Types of heterostructures

junctions are: (A) p-n homojunction: In this junction, a semiconductor interface of the same semiconducting material, and band gap but of different doping types is used. In most cases, n-type and p-type materials play the role of donor and acceptor, respectively. (B) p-n heterojunction: An interface between two dissimilar semiconductors with unequal band gaps. A heterojunction structure for better charge separation at the interface between two semiconductors. Semiconductor interfaces can therefore be organized into three types of heterojunction, as shown in Fig. 10.2.

(a) Straddling gap: Type I, in this case, the photogenerated electrons and holes drift from semiconductor X to Y, which causes charge recombination due to the large accumulation of the electron/holes. In this heterostructure, the charge carriers make the quantum wells in both bands.

(b) Staggered gap: Type II in which holes photogenerated on semiconductor X are supplied to semiconductor Y, and photogenerated electrons in semiconductor Y are transferred to semiconductor X for charge separation. In this heterostructure formation of a quantum well in one band and an energy barrier in the other band. Generally, the type-II heterojunction includes type-II, Z-Scheme, and S-Scheme. In the Z-scheme heterojunction, the electron transfer occurs from the higher CB of one semiconductor to the lower VB potential of the other semiconductor due to the large driving force [54]. S-Scheme heterojunction is similar to the type-II heterojunction. But both are completely different due to the charge-transfer path. In the case of type II, photoelectrons and holes are accumulated on the CB of the oxidation photocatalyst, and VB of the reduction photocatalyst, respectively, in the weak redox ability. But for the S-Scheme, it is vice-versa [101].

(c) Broken gap: Type III, in this heterojunction, there is no directional transport of photogenerated carriers between the semiconductor X and Y. The type-III heterojunction is identical to that of the type-II heterojunction, with the exception that the severe staggered gap prevents the band gaps from overlapping. Therefore, the type-III heterojunction is not ideal for boosting the separation of electron–hole pairs because electron–hole

migration and separation between the two semiconductors cannot occur [111].

(iii) **Water splitting and redox reaction**: The electric field that is already present can separate the photogenerated charge. At the photoanode, the photo-excited electrons are collected via the back contact and channelized to the counter cathode, wherein the protons are reduced to H_2. At the same time, holes migrate to the surface of the photoelectrode for an OER. In the case of a photocathode, the HER is carried out by driving the electrons to the surface of the electrode. The splitting of water is a non-spontaneous reaction and requires a Gibbs' free energy of 237.2 kJ/mol under the ideal conditions of 1 mol ion concentration, 1 atm gas pressure, and 25 °C temperature. This value corresponds to a theoretical thermodynamic reversible potential of 1.23 V. The Nernst equation states that the value of the potential changes with the pH of the electrolyte according to the relation: $E_{RHE} = E_{NHE} + 0.059pH$, where E_{RHE} is the potential w.r.t reversible hydrogen electrode, and E_{NHE} is the potential in relation to a normal hydrogen electrode.

10.4 Nanomaterials as Photoelectrocatalyst

At the nanoscale dimension, the scattering rate is greatly reduced, and carrier collecting efficiency is increased as their diameter is equivalent to carrier scattering lengths. Thus, nanomaterials have substantial absorption coefficients due to the rise in oscillator strength, enabling great conversion efficiency. The nanomaterial's band gap (QDs and semiconductors) can cover the entire solar spectrum and alter the absorb specific wavelengths by changing their size. Further, with the help of doping the electronic band structure and heterostructure can be modified. Moreover, it enables rapid charge transfer and mass, enhanced light absorption, and reduced dispersion of light. The photocatalytic activity can be increased by coating the electrode with nanoparticles or dispersing them in the water used as the reaction medium. In the case of PEC, the basic idea is to convert solar energy into hydrogen by applying an exterior bias to a photovoltaic material dipped in an electrolyte. When using the reference electrode to do measurements, one vital understanding in a PEC system is knowing the Fermi Energy (E_f), which compares the E_f of the semiconductor with its own constant Fermi level. The probability of discovering an electron at this energy level is cut in half. In an intrinsic semiconductor, E_f lies exactly between E_c and E_v or at the center of the band gap. Depending on the kind of dopant, E_f moves closer to or farther away from Ec. Equilibration occurs at the interface by adjusting the semiconductor's Fermi Level to match the redox couple of the electrolyte. Depending on the type of semiconductor (n-type/p-type), this creates a small region of space charge layer near the semiconductor surface that bends the band up or down [75]. To put it simply, increasing the effectiveness of water splitting is highly dependent on the photoelectrodes' electrical characteristics. It has been demonstrated that it is difficult to optimize every process in a single component. Numerous efforts have been

made to increase effectiveness and absorb a broad spectrum of light including the construction of photocatalysts with heterostructures (n–n/n-p/p-p transitions) [60]. In this direction, several classes of materials have been investigated as photoelectrodes, including metal oxide semiconductors, metal-doped semiconductors, nitrides and carbides. The 2D materials are usually composed of sturdy covalent bonds and weak Van der Waals bonds, which lead to stability of in-plane and stacked layer structure formation, respectively.Trailing the breakthrough of graphene (2004), a new perspective opened for investigating other 2D materials, for example, transition metal oxides (TMOs), transition metal dichalchalcogens (TMDs), graphene, and MXenes [6].

10.4.1 Factors Affecting the PEC Efficiency of 2D Nanomaterials

The orderliness, homogeneity, and morphology of the catalysts heavily influence their performance and efficiency in water splitting. Controlling the shape and the structure, in addition to shrinking the size, is crucial for an effective mechanism for splitting water, and the same are discussed below.

10.4.1.1 Crystallanity

When compared to amorphous materials, highly organized crystalline materials perform substantially better. Such as, the photocurrent characteristics of crystalline/annealed TiO_2 nanotubes are greater than the amorphous TiO_2 nanotubes. At a high temperature of around 300 °C, amorphous TiO_2 nanotubes are capable of crystallization. It is evident that a structural attribute can affect the photocurrent efficiency as the number of defects and the site for e/h + recombination decreases as crystallinity increases. The e/h + transfer and OER/HER reactions of semiconductors depend heavily on the crystallinity and surface-active sites, respectively. High crystallinity materials with few flaws can reduce the recombination of e/h^+. OER/HER reactions should proceed more quickly than backward reactions, which mostly depend on the quantity of active sites [28]. Shi et al. showed that high-temperature annealing (540 °C) improved the crystallinity of the $BiVO_4$ film, which reduced the electron–hole recombination and boosted PEC water splitting when exposed to light [87]. By Kim et al. showed the efficiency of the PEC water splitting was also discovered to be directly enhanced by enhancing the crystallinity of the produced photoanodes [48].

10.4.1.2 Dimensionality

Based on their dimensions, nanomaterials can be divided into 0D, 1D, 2D, and 3D structures. In which 2D nanostructures such as TiO_2 thin films [40], MoS_2 nanosheets

[105], hematite films, and g-C_3N_4 [62] nanosheets are utilized for the oxidation in PEC water splitting processes. It can effectively harvest a significant amount of UV radiation because of its thin profile and substantial surface area, which in turn can increase hydrogen generation efficiency by enabling charge transfer onto the surface. Compared to thin films, nanorods and nanowires transfer charge carriers more effectively and are more photoactive. Nanotubes have a higher surface area than nanorods and nanowires, allowing for a faster redox reaction rate even when only a small portion of them are exposed to light absorption [45].

10.4.1.3 Band Gap

The ability to precisely tune the band gap is nanomaterials' main benefit. The band gap's narrowing is thought to improve the PEC's characteristics. This aids in the vast range of solar spectrum absorption. Large band gaps cannot absorb the requisite intensities of light energy to divide the water effectively. For effective PEC water splitting, the band gap should be between 1.6 and 2.2 eV. The band edge position is exact, and the mobility of the photogenerated charge carrier is enhanced in this band gap range. Donor–acceptor can be included in the semiconductor to reduce the band gap. Band edge position and carrier diffusion length are important factors when choosing a suitable material. In contrast to the H_2 formation potential, CB should be more negative, and VB should be more favorable than his O_2 formation potential [98].

10.4.1.4 pH Dependency

PEC cells work in a variety of pH environments. The pH of the electrolyte measures whether the net charge adsorbed on the surface is positive, negative, zero, or and has a large impact on the equilibrium of the water-splitting reaction [45]. To ensure efficiency, photo corrosion of the electrode should be minimized even under hard and corrosive electrolytic conditions. The electrode surface may become less durable due to ion migration occurring during reactions. Photoelectrodes with nanomaterial integration display stability under various pH settings. Buffering the electrolyte solution increased the photocatalytic stability and property [21].

10.4.1.5 Size

The performance of PEC can be improved with the help of co-catalysts' size effects. One method to increase PEC efficiency is to create a good catalyst. The electro kinetics, which results in increased electron–hole recombination, dominates in smaller particles. Greater charge extraction at the electrode and electrolyte interface is possible due to the band-bending features of larger particles. It follows that larger cocatalysts are suitable for greater PEC performance [76].

10.4.1.6 Temperature and Pressure

Temperature is a key factor in improving PEC effectiveness. Experiments are frequently carried out in hot environments. Low temperature treatments exhibit increased PEC efficacy in a study. When the temperature was low, the incident photon to current efficiency (IPCE) rose by up to 95%. Researchers found that increasing working pressure improves the band gap [2].

10.4.1.7 Type of Pollutants

The co-existence of organic substances and heavy metals complicates the situation due to their complex interactions as compared to a single pollutant [104]. Numerous studies have shown that PEC performs better treating individual pollutants that can be organic and heavy metals. Chen et al. showed the removal of Cu-EDTA mixture (pH 3.18) by photolysis and electrocatalysis techniques. These methods demonstrate a low removal rate of pollutants at a current density of 0.5 mA/cm^2 while PEC achieved approx. 74% removal of Cu-complex and 75.54% recovery of Cu(II) recapture, indicating its potential over PC and EC [16]. A similar behavior of PEC treatment is reported by Wang et al. [97] for the treatment of mixed (organic-metal). Operation variables such as the applied bias potential or current, the solution pH, the concentration of organic-heavy metal mixed pollutants, the type of electrolyte and the electrolyte concentration reveal notable influence in the PEC removal of these pollutants [38]. The authors presented evidence of effect of pH; an increasing trend in pollutant removal was observed when pH was varied from 10.0 to 3.0. Similarly, Zhao et al. [113] showed the influence of the initial concentration of pollutants on PEC activity. It happen due to a limited amount of photogenerated holes and OH oxidants.

10.4.2 Synthesis Methods for 2D Photoelectrodes

2D materials can be synthesized via the hydrothermal route, sol–gel method, co-precipitation, and impregnation methods, as shown in Fig. 10.3. Table 10.1 also lists the synthesis approach of various 2D photoelectrodes. A brief discussion about each method is discussed below:

10.4.2.1 Hydrothermal Synthesis

Hydrothermal synthesis is a straightforward and practical method for fabricating semiconductor photocatalysts with high purity [51, 78, 100, 102]. Substances from the precursors are first added to distilled water, agitated for a while, placed in the stainless steel autoclave (Teflon-lined) and heated up to ~220 °C for several hours

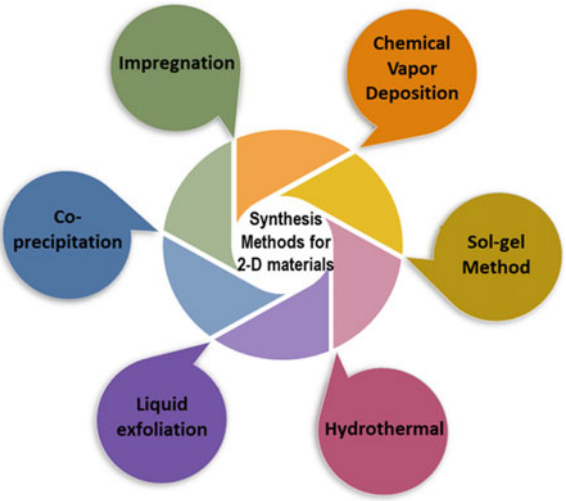

Fig. 10.3 Various methods for the synthesis of 2D materials

[8]. If non-aqueous chemicals are used as a solvent in place of water, the technique is known as solvothermal synthesis [59]. This is a typical technique that has been frequently utilized to synthesize 2D nanomaterials [100, 102]. A generalized solvothermal approach is shown by Dou et al. [20] for the assembly of several metal oxide nanosheets, including ZnO, TiO_2, MnO_2, Co_3O_4, Fe_3O_4, and WO_3. These metal oxide nanosheets ranged in thickness from 1.6 to 5.2 nm, or layers of 2- 5 stack forming the monolayer. Additionally, ZnS, ZnSe, CeO_2, and In_2O_3 were among the non-layer structured 2D nanosheets that Xie and co-worker [50, 93, 94] developed using the hydro/solvothermal approaches.

10.4.2.2 Sol–gel Synthesis

The sol–gel method is a widely used technique for the fabrication of photoelectrodes. This procedure has the potential to take care of the surface and textural parameters of the catalysts [74]. This technique is among the easy-to-process and most efficient techniques for engineering different nanomaterials [53]. In order to obtain the appropriate chemical composition, nanostructure, and surface characteristics, Parashar et al. [73] investigated stable and effective sol–gel synthesis protocols of TiO_2, SnO_2, WO_3, and ZnO nanomaterials. Along with that, Panimalar et al. [72] reported the successful fabrication of MnO_2/g-C_3N_4 hybrid nanocomposites via the facile sol–gel method with a combination of annealing. Compared to physical approaches, the sol–gel pathway is more cost-effective since it uses low operating temperatures and less energy [80].

Table 10.1 Various material syntheses methods for 2D photocatalyst

S/n	Photocatalyst material	Precursors	Synthesis process	References
1	NiMnLDHs/g-C_3N_4	$Ni(NO_3)_2.6H_2O$, $MnCl_2.4H_2O$ and dicyandiamide	Hydrothermal method	[84]
2	Nb_2O_5/ZnAl LDHs	$Zn(NO_3)_2.6H_2O$, Al $(NO_3)_3.9H_2O$	Hydrothermal method	[41]
3	Bi_2O_3/Bi_2WO_6/MgAl	$MgSO_4{\cdot}7H_2O$, Al $(NO_3)_3{\cdot}9H_2O$ and $Bi(NO_3)_3{\cdot}5H_2O$	Hydrothermal method	[7]
4	MnO_2/g-C_3N_4	Urea, Potassium permanganate ($KMnO_4$), Manganese (II) sulfate ($MnSO_4.H_2O$)	Sol–gel method	[72]
5	Mo_2C/graphene	Gold foil, Mo foil, CH_4	CVD	[92]
6	Graphene/Cu foil	Copper foils, a mixture of methane and hydrogen	CVD	[52]
7	MoS_2/SiO_2/Si	MoO_3 and S powders	CVD	[49]
8	WS_2	Tungsten (IV) disulfide, poly(vinylidene fluoride) (PVDF), copper foil, acetone and ethanol	Liquid exfoliation	[18]
9	ZnAl/g-C_3N_4/CuO	$Al(NO_3)_3{\cdot}9H_2O$, $Zn(NO_3)_2{\cdot}6H_2O$, melamine and $Cu(O)_2{\cdot}H_2O$	Co-precipitation method	[63]
10	g-$C_3N_4/SnIn_4S_8$	Tin (IV) chloride pentahydrate ($SnCl_4{\cdot}5H_2O$), indium (III) chloride tetrahydrate ($InCl_3{\cdot}4H_2O$), Dicyandiamide and urea	Co-precipitation method	[47]
11	Bi_2WO_6	Bi_2WO_6, 8.3416 g of $Bi(NO_3)_3{\cdot}5H_2O$, $(NH_4)_{10}(W_{12}O_{41}){\cdot}H_2O$ and HNO_3	Co-precipitation method	[3]
12	MoS_2/CdS	$(NH_4)_2MoS_4$, Commercial CdS powder	Impregnation method	[120]
13	WS_2/CdS	Commercial CdS powder, $(NH_4)_2WS_4$	Impregnation method	[121]

10.4.2.3 Chemical Vapour Deposition (CVD)

Another intriguing way to grow high-quality single crystalline 2D sheets on substrates is the CVD technique [42, 88, 91]. It allows adjustable thickness, scalable size, and outstanding electrical characteristics of grown material. At temperatures as high as

1000 °C, Li et al. [52] used a variety of methane and hydrogen to grow graphene using carbon by CVD on copper foils. Additionally, Shi et al. utilize MoO_3 and S powders as the reactants to fabricate the MoS_2 layer through CVD directly on SiO_2/Si substrates [88]. However, the downside of the CVD process is that it requires particular substrates, high temperatures, and high vacuums.

10.4.2.4 Liquid Exfoliation

The process of liquid exfoliation consists of the sonication of multilayer bulk crystals in surfactant/polymer solutions that result in high yield and industrial scale production of ultrathin 2D nanomaterials [36, 65, 117]. Though, this approach produces a low yield of single-layer sheets along with the challenge of dissociating the monolayer sheets from the mixture. As a substitute, the ion-intercalation and exfoliation approach was established to fabricate monolayer nanosheets at high yield and on a large scale, including graphene, MoS_2, WS_2, TiS_2, ZrS_2, and others [18, 109, 110], Castellanos-[10]. The 2D Nanosheets produced by this method have several flaws and limited lateral size [114]. Additionally, this technology is extremely susceptible to oxidation.

10.4.2.5 Co-precipitation Technique

The co-precipitation technique is a frequently used method to fabricate various nanomaterials, including semiconductor-based composites [58]. It is a very facile method to synthesize iron oxide nanoparticles (Fe_3O_4 or γ-Fe_2O_3) specifically [26]. This technique is mostly utilized for developing mixed oxides [43]. García-Pérez et al. [25]utilized the co-precipitation process for the formation transition metal tungstates having the typical formula $M^{2+}WO_4$ (M^{2+} = Co, Cu, Mn, and Ni) and studied their photocatalytic activity [25]. In another work, Kianpour et al. claimed the first low-temperature co-precipitation approach for the development of g-C_3N_4/$SnIn_4S_8$ material in their work [47]. However, this approach does not perform effectively if the reactants have significantly varied precipitation rates [79].

10.4.2.6 Impregnation Method

This method allows the final characteristic and structure to be controlled in advance as well as efficient and stable. The amount and heating of the precursor are two factors that have an impact on the impregnation technique-synthesized composites [31]. In regard to this, Zong et al. developed TMD-based photocatalysts, including MoS_2/CdS [119] and WS_2/CdS [121] that showed strong photocatalytic activity by impregnating host materials with TMD precursors and high-temperature calcination. However, obtaining precise shapes and layer-number controlled with this method is

very challenging. Additionally, the material aggregation brought on by high temperatures may result in a reduction in the specific surface area and active catalytic sites [120].

10.5 2D Nanomaterials in a Dual PEC System

10.5.1 Metal Oxide Semiconductors

Single TMOs are highly widely employed as photocatalytic semiconductors due to their exceptional chemical stability and efficiency. TiO_2 and ZnO are prominent catalysts for waste degradation and hydrogen production [22, 35, 106]. The conduction and valance band edge potentials of TMOs (as described in Fig. 10.4) are beneficial for a diversity of applications involving water splitting and pollutant treatment by thermodynamical aspect [33]. Though, due to their extensive optical bandgaps of 3.2–3.4 eV only the UV region of the solar spectrum is available for light absorption [23]. Thus, TMOs, which comprise significantly lesser bandgap and absorb visible light, are highly needed. TMO like WO_3, MoO_3, and V_2O_5 consist of a bandgap between 2.6 and 3.0 eV that can absorb light in a visible area. Along with that, they show better electron transport traits, so there will be a decrease in the fast charge recombination, which is otherwise a frequent demerit of TMOs [15, 44, 67]. A unique PEC reactor was designed by utilizing TiO_2 by Ghassan Chehade et al. to produce hydrogen and treat the waste product of galvanizing industry [11]. This unique reactor design enables chlorine gas evolution at the surface of the photoanode without dissolution and hydrogen gas to flow out of the reactor through the cathode compartment having aqueous 5 M HCl as an electrolyte. An excellent proton and H^+ transfer rate are also enhanced by this innovative design of the corrosion-resistance cathode, while the photoanode improves the charge transfer process. The reactor is used for the PEC studies with and without sunlight. It showed the generation rate of hydrogen was 3 ml/min [11]. Similarly, T.T. Guaraldo et al. studied $Ti/TiO_2/WO_3$ electrodes as photoanode fabricated via electrochemical anodization and cathodic electrodeposition for simultaneous hydrogen production and dye degradation [29]. The photocurrent density of 11 mA/cm^2 was achieved with a hybrid electrode, while it was 8 mA/cm^2 in the case of pristine TiO_2. The hydrogen production efficiency attained was 46%, while an 85% reduction in TOC was observed [29]. In another work by Ouyang et al., $BiVO_4/WO_3$ is utilized as a photoanode, and MnO_2/graphene oxide (GO) hybrid was used as a cathode [68]. The inverse opal-shaped photoanode ($BiVO_4/WO_3$) attained a photocurrent density of ~5.04 mA/cm^2, which was greater than bare material at 1.2 V versus Ag/AgCl. The inverse opal $BiVO_4/WO_3$ photoanode was merged with the improved cathode (MnO_2/GO) to design a visible-light accessible PEC system. The modified system indicated better photocurrent generation of 593.5 mA/cm^2 compared to only

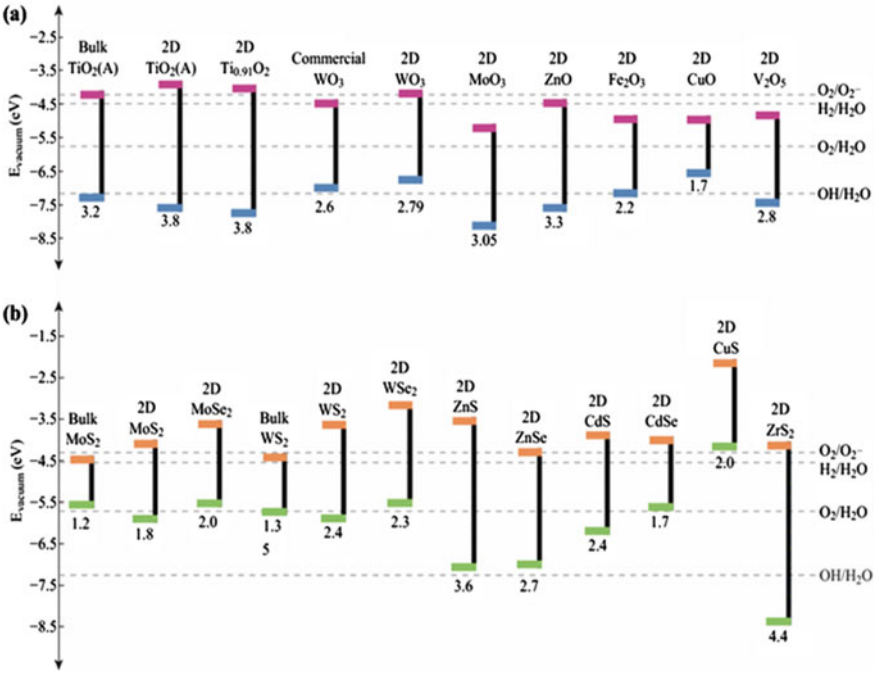

Fig. 10.4 Band structure of **a** TMOs and **b** TMDs (Reproduced with permission from [33])

MnO_2 cathode, i.e. 255.9 mA/cm^2. Additionally, Rhodamine B degradation was also confirmed for successfully establishing pollutant degradation application [68].

10.5.2 Transitional Metal Dichalcogenides

Transition metal dichalcogenides are also studied due to their earth abundance [39]. The TMDs like MoS_2, $MoSe_2$, WS_2, and $TiSe_2$ shown in Fig. 10.4 are a group of layered substances with typical formula of MX_2, where M is an element from transition metal group 4–10, e.g. Ti, Zr, V, Hf, Nb, Ta, W, Mo, and X is the from chalcogens like S, Se, and Te [17, 20]. For PEC applications, TMD nanosheets can be utilized by various means i.e. by boosting light absorption in the visible part of the solar spectrum, as a photosensitizer, as a charge separator via band alignment, and charge transporter [13, 37, 96, 112, 115].

Chen et al. studied a sequence of direct Z-scheme by synthesis of $MnIn_2S_4$/g-C_3N_4 photocatalysts via hydrothermal route as a result of in-situ stocking of $MnIn_2S_4$ flakes on the top of g-C_3N_4 nanosheets [12]. To achieve high efficiency for the simultaneous degradation of pharmaceutical wastewater and hydrogen generation, the weight ratio between $MnIn_2S_4$ nano-flakes and mesoporous g-C_3N_4 nanosheets

was optimized. The development of Z-scheme $MnIn_2S_4$/g-C_3N_4 structures efficiently enhanced the transfer and estrangement of photogenerated charge carriers via close interface connections established between these two materials. The good stability of $MnIn_2S_4$/g-C_3N_4 nanocomposites was demonstrated by re-utilization of it for pharmaceutical wastewater treatment [99].

Zheng et al. proposed a multifunctional PEC procedure for the instantaneous degradation of pharmaceuticals and personal care products (PPCPs), generation of H_2 and disinfection of *E. coli* based upon MoS_2@BL-$BiVO_4$ photoanode [116]. An improved MoS_2@BL-$BiVO_4$ photoanode (Fig. 10.5) with decreased recombination of surface charge was fabricated that showed enhanced photocurrent density (2.21 mA/cm^2) in real sewage water, which was 8.1 times higher of pristine $BiVO_4$. The hybrid photoanode attained absolute removal of 2 ppm benzophenone-3, along with 89.32 μmol of hydrogen production and decontamination of *E. coli* bacteria in a time limit of 30 min at a bias of 1.0 V versus Ag/AgCl. The PEC system exhibits outstanding reusability and stability while degrading PPCPs with reasonable efficiency [116].

10.5.3 Graphene and Graphene like Materials

Graphene is a monolayer of sp_2-bonded carbon atoms, wherein each carbon atom is a surface atom, giving the material a large exposed area and p-conjugated structure. Graphene frequently exhibits remarkable electrical and thermal conductivities due to its honeycomb-like organizational structure and one layer of carbon atoms arranged in a 2D hexagonal lattice. These properties enable graphene sheets to accept and transport excited semiconductor electrons efficiently, decrease charge recombination, improve charge transfer at interfaces and photocatalytic reaction centres and provide extra active adsorption sites. and enhance the production of photocatalytic H_2 activity [45].

Graphene oxide (GO) is an oxidized form of graphene that has oxygen-containing functional groups that are advantageous. Examples include carbonyl, hydroxyl, carboxyl, and epoxy groups. Graphene is easier to functionalize with other user groups even though it is more conductive than reduced GO (rGO). Natural remediation is one of the many domains where graphene-based materials have inspired research [66].

Graphene-based materials are beneficial due to their high bonding density and oxygen-containing functional groups. Every graphene-based substance has a significant surface area. Graphene-based nanomaterials may act as adsorbents via hydrogen bonds, pie-bonds, hydrophobic, electrostatic, and covalent interactions, among other conceivable interactions. Thus, materials made of graphene are effective at absorbing many types of pollutants from water. A nanostructured composite $FeMoO_4$-GO catalyst synthesized via a simple one-pot hydrothermal technique is reported as a superior electrode with high degrading capacity and quick hydrogen generation rates. The electrode could perform 90% of berberine elimination within 30 min. At a

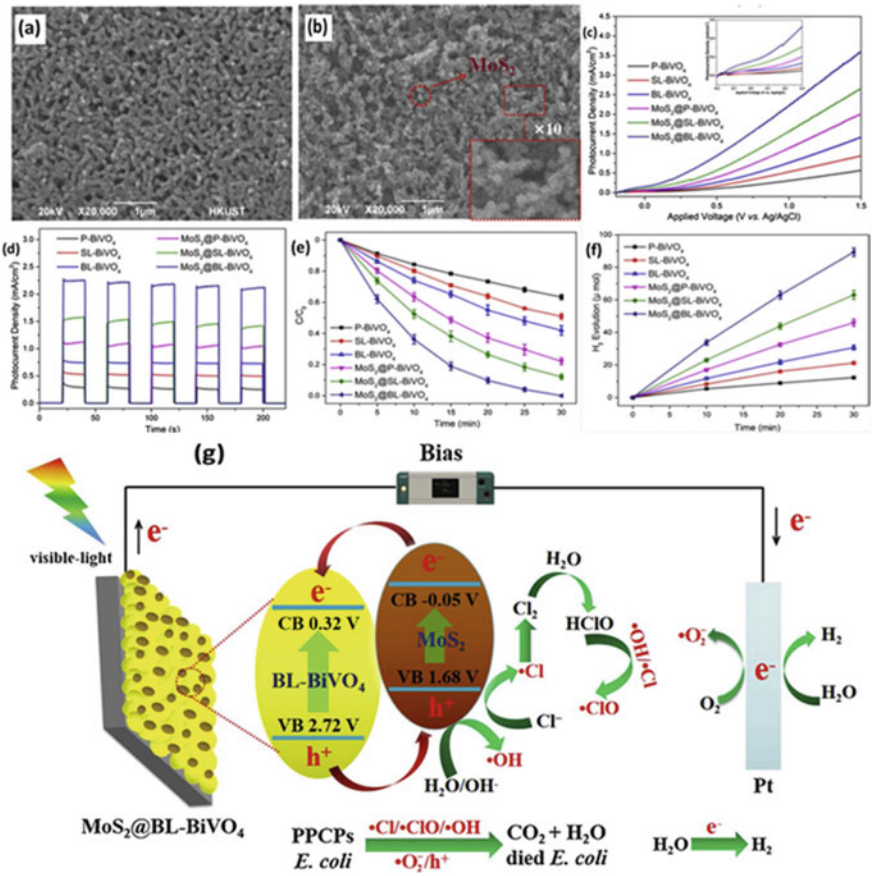

Fig. 10.5 **a** SEM image of BL-$BiVO_4$, **b** hybrid MoS_2@BL-$BiVO_4$, **c** Linear sweep voltammetry (LSV) graph and **d** transient photoresponse of the photoanodes in the sewage at 1.0 V versus Ag/AgCl applied, **e** degradation of BZP, **f** H_2 generation using various photoanodes at 1.0 V versus Ag/AgCl in real sewage water. **g** schematic diagram showing the process of multifunctional system for removal of PPCPs, disinfection of *E. coli* and generation of H_2 in sewage by MoS_2@BL-$BiVO_4$ hybrid electrode. (Reproduced with permission from [116])

current density of 10 mA cm^{-2}, the fabricated system generated hydrogen at a rate of 3.1 mmol cm^{-2} min^{-1} [95]. In another work by Hongqiang Shen et al., a two-step solvothermal fabrication process was used to create a 2D/2D/3D Z-scheme system of Cu_2O/RGO/$BiVO_4$, which could not only produce H_2 but also degrade TC simultaneously [86]. An attempt is also made by fusing the optoelectric properties of AgNPs with those of MoS_2/RGO/$NiWO_4$ (Ag-MRGON) heterostructures to design a Z-scheme-based photosystem with enhanced light absorption capacity. The applied bias to photocurrent efficiency (ABPE) is reported as 0.52% and 17.3 times, and 4.3 times better than the pure MoS_2 and MoS_2/$NiWO_4$ photoanode, respectively. The photocurrent density of Ag-MRGON was increased to 3.5 mA/cm^2 and the charge

recombination was controlled using AgNPs as photo enhancers and RGO as electron mediators to reach photo stability of about 2 h. Furthermore, the photocurrent onset potential of the Ag-MRGON heterojunction (i.e., 0.61 V_{RHE}) cathodic was reduced in comparison to $NiWO_4$ (0.83 V_{RHE}), MoS_2 (0.80 V_{RHE}), and $MoS_2/NiWO_4$ heterojunction (0.73 V_{RHE}). In similar lines, a hybrid nanostructures of $BiVO_4$/Ag/rGO is shown for improved PEC-WS performance over $BiVO_4$. The system exhibited an IPCE of 3.5% and solar to hydrogen (STH) of 0.9% and was successful in degrading MB and phenol [34]. Another hydrothermally synthesized Z-scheme system $ZnIn_2S_4$/RGO/$BiVO_4$ was shown hydrogen production and simultaneous organic pollutant degradation. The organic contaminants can encourage the production of hydrogen from the breakdown of water. The hydrogen production rate, formaldehyde degradation rate, apparent quantum yield (A.Q.Y.) and the n_c are calculated to be 1687 mol g^{-1} h^{-1}, 22.2 mmol g^{-1} h^{-1}, 22.9%, and 13.3%, respectively, at a formaldehyde concentration of 5 mol l^{-1}, catalyst concentration of 1.5 g l^{-1} and pH 13 [118]. The system can also have good activity for hydrogen production and organic pollutant breakdown when mixed organic pollutants are supplied.

Similarly, Wei et al. worked on the synthesis of bismuth-doped g-C_3N_4 nanohybrid through a two-stage solvothermal technique. In accordance with the concept of turning waste into energy, efficiencies were quantified by measuring the evolution of hydrogen from antibiotic wastewater. The optimized sample (Bi/g-C_3N_4) showed 35.9 μmol/h of H_2 evolution rate under visible light that is about three times of bare g-C_3N_4. Results showed that it is possible to combine hydrogen evolution with concurrent antimicrobial wastewater degradation. Additionally, the samples displayed excellent stability throughout cycling tests after being zanalyzed by XRD and XPS descriptions [99].

The mixture of graphene and these hybrids can enhance the unique qualities of graphene and produce new qualities, such as effective charge separation and transfer properties, in addition to excellent stability, which can increase the overall photocatalytic efficiency in water splitting for the production of O_2 and H_2 [100, 102]. However, several obstacles still exist, even though significant advancement has been made recently. First off, the microstructure of the graphene and TMDCs composites plays a significant role in determining their properties and uses. Therefore, the composites must be designed with great caution to achieve great quality, high equivalent morphology on the nanoscale and better photocatalytic capabilities. Second, the absence of hydrophilic functional groups on pure graphene sheets presents significant hurdles for the fabrication of graphene-based nanomaterials or high-quality graphene. As a result, it is important to improve suitable reduction processes to lessen flaws in graphene sheets while maintaining their conductivity. Thirdly, in TMDCs materials with low coordination, the atoms near the grain boundaries or edges are usually very active for electrochemical interaction. However, the density of active sites and inadequate electronic transport severely restrict their electrochemical activity. To get around these restrictions, TMDCs with extremely active sites must be zsynthesized and zhybridized with extremely conductive materials like graphene. Last but not least, it is not entirely clear how adding graphene, and TMDCs improves photocatalytic performance. Therefore, effective fusion of theoretical calculations and actual

results will necessitate several investigations to grasp the enhancing mechanism of graphene-based composite photocatalysts in wastewater treatment and hydrogen generation [46].

10.5.4 MXenes

With the discovery of a new class of 2D materials, MXenes, several reports have been obtained on the increased PEC efficiency of the photocatalysts containing them. This is because the 2D layered structure of MXenes can expose multiple unsaturated metal sites (for example, Ti, Nb, or V), leading to higher redox reactivity than single elemental carbon materials [107]. Moreover, the hydrophilic functional groups (such as - $^{-}$OH, F and O) present on the surface of MXenes are advantageous for binding to various device components such as semiconductors and the long-term stabilization of 2D MXenes in aqueous solution [24]. MXene also possesses strong metallic conductivity, which, like graphene, also contributes to efficient charge transfer. Due to the MXene family's exceptional features, 2D MXenes are prospective building blocks for effective photoelectrodes. Monolayer MXene has a hexagonal lattice with a rhombohedral unit cell, similar to graphene in the top view. However, MXene materials that function as HER electrodes need a large overpotential to split water.

Consequently, a workable solution to address this problem is to integrate MXene photoelectrode with other functional components [46]. MXene hybrids are highly suitable for PC/PEC water splitting to capture sunlight due to their effective H^+ adsorption, suitable EC water splitting capacity, and close matching of Fermi energy (E_F) positions with H^+/H_2 reduction potentials. PC processes, in contrast to EC, demand semiconductor photo absorbers, whereelectron–hole pairs are produced. Therefore, other photoactive materials must be combined with MXenes since most MXenes are metallic and not semiconducting.

Lately, nano carbons have been incorporated into MXene-based systems to enhance interfacial bonding, increase photogenerated charge carrier separation and improve injection efficiency. These results indicate that 2D-MXene/Nano carbons are one of the most promising materials for photoelectrodes in PEC systems for effective renewable energy conversion. But, 2D-MXenes still lack the expected photo response to generate photo-induced electrons and holes, which is important for photovoltaic PEC-HERs, and thus nowadays researchers are finding for 2D-MXene/nanocarbon photocathodes. Further progress in PEC-HER activities is needed.

Due to the excellent metallic conductivity of 2D MXenes/nanocarbons, it is necessary to add photoactive components to create triad photocathodes by interacting with them as cocatalysts. MXene hybrids have been used as versatile PEC-HER, OER, and water-splitting catalysts in several publications. Lin et al. reported a $Ti_3C_2T_x$/InGaN photoanode with a tenfold increase in HER photocurrent density with the addition of MXene, confirming the significant HER activity on the MXene surface [57].

The TTL($Ti_3C_2T_x$/TiO_2/NiFeCo-LDH)/$BiVO_4$ photoanode presented a much better photocurrent density of 2.25 mA /cm^2 at 1.23 V (vs. RHE) in comparison to the pristine $BiVO_4$ (0.39 mA/cm^{-2}) in the potential range of 0.2 to 1.4 V (vs. RHE), which is about five times more than the pristine $BiVO_4$ [32]. A $Ti_3C_2T_x$ system is shown in combination with TiO_2 as an efficient photoanode over bare TiO_2. The $Ti_3C_2T_x$/TiO_2 as an OER photoanode exhibited a sixfold increase in the ABPE. The photoanode Ti_3C_2/TiO_2 showed a super high photocurrent density of 1.94 mA/cm^2 at 1.23 V versus RHE, which is six times higher than bare TiO_2 [14]. The MXene surface functioned as a hole scavenger and OER active site in this instance, where PEC OER took place [55]. MXenes are primarily used as conductive supports and electronic modulators since, as previously mentioned, they typically only have minimal OER activity. As a result, they must be zhybridized with OER-active catalysts (such TMDC and LDHs) to produce OER. To benefit from MXenes' HER activity, most PC/PEC applications for MXenes and their hybrids are focused on HER rather than OER. However, MXene systems are not yet studied in wastewater environments for simultaneous treatment and hydrogen generation, which requires detailed study to establish their potential in this domain.

10.6 Conclusions and Future Prospective

In the last decade, the utilization of 2D materials have been established for the PEC treatment of wastewater and the production of hydrogen simultaneously. These PEC studies showed the effects of pH, kind of electrolyte, applied bias, and pollutant content-like variables at the rate of hydrogen generation and removal efficiency of pollutants which confirmed the requirement of optimization in the fabrication of 2D photocatalysts. Due to solar energy's renewable significance, research on light sources has steadily shifted from ultraviolet (UV) to visible light and sunshine. The fabrication of several nanostructured, doped and composite semiconductor electrodes like TMOs, TMDs, graphene and MXenes with improved ability made it possible to absorb visible light and utilize solar energy. However, irrespective of the good performances of laboratory-level experimental outcomes, further research is certainly required to improve PEC technology to remove pollutants and produce hydrogen at an industrial scale. The development of extremely effective large-scale photocatalysts and fabricating adaptable PEC reactors according to real samples is still a challenge that needs the focus of researchers. Also, there is a need to develop hybrid 2D materials which can absorb near-infrared light that cover the largest area of the sun-spectrum. There is no question that PEC's forthcoming studies on wastewater management will be crucial, but there is still a long way to go. It is expected that the PEC technique can successfully use solar power to simultaneously treat pollutant wastewater and generate hydrogen on industrial scale.

Acknowledgements Authors are thankful to Director, CSIO for his kind permission. The funding support under SERB WEA Project WEA/2020/000022 is highly acknowledged. PS and SS are thankful to GATE-JRF and DST INSPIRE, respectively for doctoral study fellowship.

References

1. A. Fujishima, K.Honda, Electrochemical photolysis of water at a semiconductor electrode. Nature **238**, 37–38 (1972)
2. F.A. Al-Agel, J. Suleiman, S.A. Khan, Studies on silicon quantum dots prepared at different working pressure. Results Phys. **7**, 1128–1134 (2017). https://doi.org/10.1016/j.rinp.2017.03.002
3. S.O. Alfaro, A. Martínez-De La Cruz, Synthesis, characterization and visible-light photocatalytic properties of Bi2WO6 and Bi2W2O9 obtained by co-precipitation method. Appl. Catal. A Gen **383**(1–2), (2010). https://doi.org/10.1016/j.apcata.2010.05.034
4. M.Y. Azwar, M.A. Hussain, A.K. Abdul-Wahab, Development of biohydrogen production by photobiological, fermentation and electrochemical processes: a review. Renew. Sustain. Energy Rev. **31**, 158–173 (2014). https://doi.org/10.1016/J.RSER.2013.11.022
5. D.S. Babu et al., Detoxification of water and wastewater by advanced oxidation processes. Sci. Total Environ. (2019). https://doi.org/10.1016/j.scitotenv.2019.133961
6. G.R. Bhimanapati et al., Recent advances in two-dimensional materials beyond graphene. ACS Nano (2015). https://doi.org/10.1021/acsnano.5b05556
7. X. Bing et al., Biomimetic synthesis of Bi2O3/Bi2WO6/MgAl-CLDH hybrids from lotus pollen and their enhanced adsorption and photocatalysis performance J. Photochem. Photobiol. A Chem. **364** (2018). https://doi.org/10.1016/j.jphotochem.2018.06.030
8. P. Blake et al., Making graphene visible. Appl. Phys. Lett. **91**(6) (2007). https://doi.org/10.1063/1.2768624.
9. E. Brown, M.W. Skougstad, M.J. Fishman, Methods for collection and analysis of water samples for dissolved minerals and gases, in *Techniques of Water-Resources Investigations 05-A1* [Preprint] (1970)
10. A. Castellanos-Gomez et al., Single-layer MoS2 mechanical resonators. Adv. Mater. **25**(46) (2013). https://doi.org/10.1002/adma.201303569
11. G. Chehade et al., A photoelectrochemical system for hydrogen and chlorine production from industrial waste acids. Sci. Total Environ. **712** (2020). https://doi.org/10.1016/j.scitotenv.2019.136358
12. W. Chen et al., Direct Z-scheme 2D/2D MnIn2S4/g-C3N4 architectures with highly efficient photocatalytic activities towards treatment of pharmaceutical wastewater and hydrogen evolution. Chem. Eng. J. **359** (2019). https://doi.org/10.1016/j.cej.2018.11.141
13. Chen, X. *et al.* (2018) 'RuII Photosensitizer-Functionalized Two-Dimensional MoS2 for Light-Driven Hydrogen Evolution', *Chemistry - A European Journal*, 24(2). doi:https://doi.org/10.1002/chem.201705203.
14. X. Chen et al., Ti3C2 MXene quantum dots/TiO2 inverse opal heterojunction electrode platform for superior photoelectrochemical biosensing. Sens. Actuators B Chem. **289**(March), 131–137 (2019). https://doi.org/10.1016/j.snb.2019.03.052
15. Y. Chen et al., Single-crystalline orthorhombic molybdenum oxide nanobelts: Synthesis and photocatalytic properties. CrystEngComm **12**(11) (2010). https://doi.org/10.1039/c000744g
16. Y. Chen et al., Photoelectrocatalytic oxidation of metal-EDTA and recovery of metals by electrodeposition with a rotating cathode. Chem. Eng. J. **324** (2017). https://doi.org/10.1016/j.cej.2017.05.031
17. M. Chhowalla et al., The chemistry of two-dimensional layered transition metal dichalcogenide nanosheets. Nat. Chem. (2013). https://doi.org/10.1038/nchem.1589

18. M.B. Dines, Lithium intercalation via n-Butyllithium of the layered transition metal dichalcogenides. Mater. Res. Bull. **10**(4) (1975). https://doi.org/10.1016/0025-5408(75)90115-4
19. M.H. Do et al., Challenges in the application of microbial fuel cells to wastewater treatment and energy production: a mini review. Sci. Total Environ. **639**, 910–920 (2018). https://doi.org/10.1016/J.SCITOTENV.2018.05.136
20. X. Duan et al., Two-dimensional transition metal dichalcogenides as atomically thin semiconductors: opportunities and challenges. Chem. Soc. Rev. (2015). https://doi.org/10.1039/c5cs00507h
21. M. Fekete et al., Photoelectrochemical water oxidation by screen printed ZnO nanoparticle films: effect of pH on catalytic activity and stability. Nanoscale **6**(13), 7585–7593 (2014). https://doi.org/10.1039/c4nr01935k
22. A. Fujishima, T.N. Rao, D.A. Tryk, Titanium dioxide photocatalysis. J. Photochem. Photobiol. C (2000). https://doi.org/10.1016/S1389-5567(00)00002-2
23. A. Fujishima, X. Zhang, D.A. Tryk, TiO2 photocatalysis and related surface phenomena. Surf. Sci. Rep. (2008). https://doi.org/10.1016/j.surfrep.2008.10.001
24. G. Gao, A.P. O'Mullane, A. Du, 2D MXenes: a new family of promising catalysts for the hydrogen evolution reaction. ACS Catal. **7**(1), 494–500 (2017). https://doi.org/10.1021/acscatal.6b02754
25. U.M. García-Pérez, A. Martínez-De La Cruz, J. Peral, Transition metal tungstates synthesized by co-precipitation method: Basic photocatalytic properties Electrochim. Acta **81** (2012). https://doi.org/10.1016/j.electacta.2012.07.045
26. R.K. Gautam, M.C. Chattopadhyaya, Functionalized magnetic nanoparticles: adsorbents and applications BT-nanomaterials for wastewater remediation, in *Nanomaterials for Wastewater Remediation* (2016)
27. D. Gielen, W. Bank, *Hydrogen: A Renewable Energy Perspective Some of the authors of this publication are also working on these related projects: A Global Renewable Energy Roadmap: Comparing Energy Systems Models with IRENA's REmap 2030 Project View project Innovation for the* (no date)
28. J. Gong, Y. Lai, C. Lin, Electrochemically multi-anodized TiO2 nanotube arrays for enhancing hydrogen generation by photoelectrocatalytic water splitting. Electrochim. Acta **55**(16), 4776–4782 (2010). https://doi.org/10.1016/j.electacta.2010.03.055
29. T.T. Guaraldo et al., On the application of nanostructured electrodes prepared by Ti/TiO2/WO3 "template": a case study of removing toxicity of indigo using visible irradiation. Chemosphere **91**(5) (2013). https://doi.org/10.1016/j.chemosphere.2012.12.027
30. J.S. Guest et al., A new planning and design paradigm to achieve sustainable resource recovery from wastewater. Environ. Sci. Technol. **43**(16), 6126–6130 (2009). https://doi.org/10.1021/es9010515
31. M. Hadnadjev-Kostic, T. Vulic, R. Marinkovic-Neducin, Solar light induced rhodamine B degradation assisted by TiO2-Zn-Al LDH based photocatalysts. Adv Powder Technol. **25**(5) (2014). https://doi.org/10.1016/j.apt.2014.05.015
32. N. Hao et al., In situ hybridization of an MXene/TiO2/NiFeCo-layered double hydroxide composite for electrochemical and photoelectrochemical oxygen evolution. RSC Adv. **8**(37), 20576–20584 (2018). https://doi.org/10.1039/c8ra02349b
33. F. Haque et al., Two-dimensional transition metal oxide and chalcogenide-based photocatalysts. Nano-Micro Lett. (2018). https://doi.org/10.1007/s40820-017-0176-y
34. A.H. Hendi et al., Visible light-driven photoelectrocatalytic water splitting using Z-scheme Ag-decorated MoS2/RGO/NiWO4 heterostructure. ACS Omega **5**(49), 31644–31656 (2020). https://doi.org/10.1021/acsomega.0c03985
35. M.D. Hernández-Alonso et al., Development of alternative photocatalysts to TiO2: challenges and opportunities. Energy Environ. Sci. (2009). https://doi.org/10.1039/b907933e
36. Y. Hernandez et al., High-yield production of graphene by liquid-phase exfoliation of graphite. Nat. Nanotechnol. **3**(9) (2008). https://doi.org/10.1038/nnano.2008.215

37. M.C. Hsiao et al., Ultrathin 1T-phase MoS2 nanosheets decorated hollow carbon microspheres as highly efficient catalysts for solar energy harvesting and storage J. Power Sources **345** (2017). https://doi.org/10.1016/j.jpowsour.2017.01.132
38. H.T. Hsu et al., Enhanced photocatalytic activity of chromium(VI) reduction and EDTA oxidization by photoelectrocatalysis combining cationic exchange membrane processes. J. Hazard. Mater. **248–249**(1) (2013). https://doi.org/10.1016/j.jhazmat.2012.12.058
39. J.S. Hu et al., Mass production and high photocatalytic activity of ZnS nanoporous nanoparticles. Angew. Chemie-Int. Edition **44**(8) (2005). https://doi.org/10.1002/anie.200462057
40. C.W. Huang et al., Hydrogen generation from photocatalytic water splitting over TiO 2 thin film prepared by electron beam-induced deposition. Int. J. Hydrogen Energy **35**(21), 12005–12010 (2010). https://doi.org/10.1016/j.ijhydene.2010.08.113
41. G. Huang et al., Nb2O5/ZnAl-LDH composites and its calcined products for photocatalytic degradation of congo red under visible light irradiation Mater. Lett. **173** (2016). https://doi.org/10.1016/j.matlet.2016.03.073
42. Q. Ji et al., Chemical vapour deposition of group-VIB metal dichalcogenide monolayers: engineered substrates from amorphous to single crystalline. Chem. Soc. Rev. (2015). https://doi.org/10.1039/c4cs00258j
43. B. Jia et al., Study of NO removal and resistance to SO2 and H2O of MnOx/TiO2, MnOx/ZrO2 and MnOx/ZrO2–TiO2. Appl. Catal. A **553** (2018). https://doi.org/10.1016/j.apcata.2017.12.016
44. H. Jiang, M. Nagai, K. Kobayashi, Enhanced photocatalytic activity for degradation of methylene blue over V2O5/BiVO4 composite. J. Alloys Compd. **479**(1–2) (2009). https://doi.org/10.1016/j.jallcom.2009.01.051
45. J. Joy, J. Mathew, S.C. George, Nanomaterials for photoelectrochemical water splitting–review. Int. J. Hydrogen Energy **43**(10), 4804–4817 (2018). https://doi.org/10.1016/j.ijhydene.2018.01.099
46. Z.B. Khalid et al., Application of 2D graphene-based nanomaterials for pollutant removal from advanced water and wastewater treatment processes. ACS Symp. Ser. **1353**(August), 191–217 (2020). https://doi.org/10.1021/bk-2020-1353.ch009
47. G. Kianpour et al., Facile synthesis and characterization of nickel molybdate nanorods as an effective photocatalyst by co-precipitation method. J. Mater. Sci. Mater. Electron. **27**(10) (2016). https://doi.org/10.1007/s10854-016-5103-3
48. J.Y. Kim et al., Charge transfer in iron oxide photoanode modified with carbon nanotubes for photoelectrochemical water oxidation: an electrochemical impedance study. Int. J. Hydrogen Energy **36**(16), 9462–9468 (2011). https://doi.org/10.1016/j.ijhydene.2011.05.046
49. N. Kumar et al., Growth of highly crystalline and large scale monolayer MoS2 by CVD: the role of substrate position. Cryst. Res. Technol. **53**(6) (2018). https://doi.org/10.1002/crat.201800002
50. F. Lei et al. Oxygen vacancies confined in ultrathin indium oxide porous sheets for promoted visible-light water splitting. J. Am. Chem. Soc. **136**(19) (2014). https://doi.org/10.1021/ja501866r
51. H. Li et al., Preparation and applications of mechanically exfoliated single-layer and multilayer MoS2 and WSe2 nanosheets. Accounts Chem. Res. **47**(4) (2014). https://doi.org/10.1021/ar4002312
52. X. Li et al., Large-area synthesis of high-quality and uniform graphene films on copper foils. Science **324**(5932) (2009). https://doi.org/10.1126/science.1171245
53. Y. Li, T. White, S.H. Lim, Structure control and its influence on photoactivity and phase transformation of TiO2 nano-particles. Rev. Adva. Mater. Sci. **5**(3) (2003)
54. G. Liao et al., Emerging polymeric carbon nitride Z-scheme systems for photocatalysis. Cell Rep. Phys. Sci. **2**(3), 100355 (2021). https://doi.org/10.1016/j.xcrp.2021.100355
55. K.R.G. Lim et al., Rational Design of Two-Dimensional Transition Metal Carbide/Nitride (MXene) Hybrids and Nanocomposites for Catalytic Energy Storage and Conversion. ACS Nano **14**(9), 10834–10864 (2020). https://doi.org/10.1021/acsnano.0c05482

56. C.Y. Lin et al., Fermentative hydrogen production from wastewaters: a review and prognosis. Int. J. Hydrog. Energy (2012). https://doi.org/10.1016/j.ijhydene.2012.02.072
57. J. Lin et al., A novel approach for achieving high-efficiency photoelectrochemical water oxidation in InGaN nanorods grown on Si system: MXene nanosheets as multifunctional interfacial modifier. Adv. Func. Mater. **30**(13), 1–11 (2020). https://doi.org/10.1002/adfm.201910479
58. J. Liu et al., ZnCr-LDH/N-doped graphitic carbon-incorporated g-C3N4 2D/2D nanosheet heterojunction with enhanced charge transfer for photocatalysis. Mater. Res. Bull. **102** (2018). https://doi.org/10.1016/j.materresbull.2018.03.010
59. Q. Liu et al., BiOCl and TiO2 deposited on exfoliated ZnCr-LDH to enhance visible-light photocatalytic decolorization of Rhodamine B. Ceram. Int. **43**(7) (2017). https://doi.org/10.1016/j.ceramint.2017.01.119
60. J. Low et al., Heterojunction photocatalysts. Adv. Mater. **29**(20), 1–20 (2017). https://doi.org/10.1002/adma.201601694
61. S.D. Melvin, F.D.L. Leusch, Removal of trace organic contaminants from domestic wastewater: a meta-analysis comparison of sewage treatment technologies. Environ. Int. (2016). https://doi.org/10.1016/j.envint.2016.03.031
62. H. Miao et al., A novel strategy to prepare 2D g-C3N4nanosheets and their photoelectrochemical properties. J. Alloy. Compd. **690**, 669–676 (2017). https://doi.org/10.1016/j.jallcom.2016.08.184
63. M. Mureseanu et al., Green synthesis of g-C3N4/CuONP/LDH composites and derived g-C3N4/MMO and their photocatalytic performance for phenol reduction from aqueous solutions. Appl. Clay Sci. **141** (2017). https://doi.org/10.1016/j.clay.2017.02.012
64. F. Murphy et al., Wastewater treatment works (WwTW) as a source of microplastics in the aquatic environment. Environ. Sci. Technol. **50**(11), 5800–5808 (2016). https://doi.org/10.1021/acs.est.5b05416
65. V. Nicolosi, (Invited) Liquid-phase exfoliated two-dimensional nanosheets: from large scale production to energy storage applcations, in *ECS Meeting Abstracts*, MA2016–01(26) (2016). https://doi.org/10.1149/ma2016-01/26/1328
66. F. Ning et al., TiO2/graphene/NiFe-layered double hydroxide nanorod array photoanodes for efficient photoelectrochemical water splitting. Energy Environ. Sci. **9**(8), 2633–2643 (2016). https://doi.org/10.1039/c6ee01092j
67. J.Z. Ou et al., Anodic formation of a thick three-dimensional nanoporous WO3 film and its photocatalytic property. Electrochem. Commun. **27** (2013). https://doi.org/10.1016/j.elecom.2012.11.009
68. K. Ouyang et al., A novel visible-light responsive photocatalytic fuel cell with a highly efficient BiVO4/WO3 inverse opal photoanode and a MnO2/graphene oxide nanocomposite modified cathode. Int. J. Hydrogen Energy **44**(14), 7288–7299 (2019). https://doi.org/10.1016/J.IJHYDENE.2019.01.241
69. M.P. Shah, A.K. Pate, Optimization of environmental parameters on microbial degradation of reactive black dye. J. Bioremediation Biodegrad. **4**(3) (2013). https://doi.org/10.4172/2155-6199.1000183
70. S. Pahra et al., A noble metal-free candle soot derived carbon electrocatalyst for simultaneous H2 generation and wastewater treatment. J. Phys. Chem. Solids **173**, 111106 (2023). https://doi.org/10.1016/J.JPCS.2022.111106
71. S. Pahra, S. Sharma, P. Devi, Fundamental understanding and figure of merits for electrocatalytic and photoelectrocatalytic H_2 production, in *Green Energy Harvesting* (2022), pp. 46–74. https://doi.org/10.1002/9781119776086.CH3
72. S. Panimalar et al., Studies of MnO2/g-C3N4 hetrostructure efficient of visible light photocatalyst for pollutants degradation by sol-gel technique. Surf. Interfaces **20** (2020). https://doi.org/10.1016/j.surfin.2020.100512
73. M. Parashar, V.K. Shukla, R. Singh, Metal oxides nanoparticles via sol–gel method: a review on synthesis, characterization and applications. J. Mater. Sci. Mater. Electron. (2020). https://doi.org/10.1007/s10854-020-02994-8

74. S.P. Paredes et al., Sol-gel synthesis of hydrotalcite-like compounds. J. Mater. Sci. **41**(11) (2006). https://doi.org/10.1007/s10853-005-5347-4
75. F. Petronella, R. Comparelli, Nanomaterials in photo (Electro) catalysis. Catalysts **11**(2), 1–4 (2021). https://doi.org/10.3390/catal11020149
76. S. Pokrant et al., Size effects of cocatalysts in photoelectrochemical and photocatalytic water splitting. Mater. Today Energy **5**, 158–163 (2017). https://doi.org/10.1016/j.mtener.2017.06.005
77. S. Popli, U.D. Patel, Destruction of azo dyes by anaerobic–aerobic sequential biological treatment: a review. Int. J. Environ. Sci. Technol. (2015). https://doi.org/10.1007/s13762-014-0499-x
78. C. Prasad et al., An overview of semiconductors/layered double hydroxides composites: properties, synthesis, photocatalytic and photoelectrochemical applications. J. Mol. Liq. (2019). https://doi.org/10.1016/j.molliq.2019.111114
79. A.V. Rane et al., Methods for synthesis of nanoparticles and fabrication of nanocomposites, in *Synthesis of Inorganic Nanomaterials: Advances and Key Technologies* (2018). https://doi.org/10.1016/B978-0-08-101975-7.00005-1
80. B.G. Rao, D. Mukherjee, B.M. Reddy, Novel approaches for preparation of nanoparticles, in *Nanostructures for Novel Therapy: Synthesis Characterization and Applications* (2017). https://doi.org/10.1016/B978-0-323-46142-9.00001-3
81. R.S. Lokhande, U.P. Singare, S.D. Pimple, Study on physico-chemical parameters of waste water effluents from Taloja industrial area of Mumbai, India. Int. J. Ecosyst. **1**(1) (2012). https://doi.org/10.5923/j.ije.20110101.01
82. S. Samsami et al., Recent advances in the treatment of dye-containing wastewater from textile industries: overview and perspectives. Process Saf. Environ. Prot. (2020). https://doi.org/10.1016/j.psep.2020.05.034
83. A.B. dos Santos, F.J. Cervantes, J.B. van Lier, Review paper on current technologies for decolourisation of textile wastewaters: perspectives for anaerobic biotechnology. Biores. Technol. (2007). https://doi.org/10.1016/j.biortech.2006.11.013
84. M. Shakeel et al., Layered by layered Ni-Mn-LDH/g-C3N4 nanohybrid for multi-purpose photo/electrocatalysis: morphology controlled strategy for effective charge carriers separation. Appl. Catal. B **242** (2019). https://doi.org/10.1016/j.apcatb.2018.10.005
85. K.P. Sharma et al., A comparative study on characterization of textile wastewaters (untreated and treated) toxicity by chemical and biological tests. Chemosphere **69**(1) (2007). https://doi.org/10.1016/j.chemosphere.2007.04.086
86. H. Shen et al., 2D/2D/3D architecture Z-scheme system for simultaneous H2 generation and antibiotic degradation. Fuel **280**(July), 1–9 (2020). https://doi.org/10.1016/j.fuel.2020.118618
87. L. Shi et al., Annealing temperature effects on photoelectrochemical performance of bismuth vanadate thin film photoelectrodes. RSC Adv. **8**(51), 29179–29188 (2018). https://doi.org/10.1039/c8ra04887h
88. Y. Shi, H. Li, L.J. Li, Recent advances in controlled synthesis of two-dimensional transition metal dichalcogenides via vapour deposition techniques. Chem. Soc. Rev. (2015). https://doi.org/10.1039/c4cs00256c
89. P. Singh et al., Recent advances in bacteriorhodopsin-based energy harvesters and sensing devices. Nano Energy (2021). https://doi.org/10.1016/j.nanoen.2020.105482
90. S. Singla et al., BiVO4/MoSe2 Photocatalyst for the photocatalytic Abatement of tetracycline and photoelectrocatalytic water splitting. Mater. Chem. Phys. **295**, 127111 (2023). https://doi.org/10.1016/J.MATCHEMPHYS.2022.127111
91. L. Song et al., Large scale growth and characterization of atomic hexagonal boron nitride layers. Nano Lett. **10**(8) (2010). https://doi.org/10.1021/nl1022139
92. W. Sun et al. Controlled synthesis of 2D Mo2C/graphene heterostructure on liquid Au substrates as enhanced electrocatalytic electrodes. Nanotechnology **30**(38) (2019). https://doi.org/10.1088/1361-6528/ab2c0d

93. Y. Sun et al., Fabrication of flexible and freestanding zinc chalcogenide single layers. Nat. Commun. **3** (2012). https://doi.org/10.1038/ncomms2066
94. Y. Sun et al., Pits confined in ultrathin cerium(IV) oxide for studying catalytic centers in carbon monoxide oxidation. Nat. Commun. **4** (2013). https://doi.org/10.1038/ncomms3899
95. L. Tang, L. Liu, F. Yang, FeMoO4-graphene oxide photo-electro-catalyst for berberine removal and hydrogen evolution. Int. J. Hydrogen Energy **44**(36), 19755–19761 (2019). https://doi.org/10.1016/j.ijhydene.2019.03.078
96. T.N. Trung et al., Enhanced photoelectrochemical activity in the heterostructure of vertically aligned few-layer MoS2 flakes on ZnO Electrochim. Acta **260** (2018). https://doi.org/10.1016/j.electacta.2017.11.089
97. H. Wang et al., Simultaneous removal of phenol and Cr(VI) by TiO2 nanotube array photoelectrocatalysis. Cuihua Xuebao/Chin. J. Catal. 32(4) (2011). https://doi.org/10.3724/SP.J.1088.2011.01246
98. J. Wang et al., Band structure tuning of TiO2 for enhanced photoelectrochemical water splitting. J. Phys. Chem. C **118**(14), 7451–7457 (2014). https://doi.org/10.1021/jp5004775
99. Z. Wei et al., Photocatalytic hydrogen evolution with simultaneous antibiotic wastewater degradation via the visible-light-responsive bismuth spheres-g-C3N4 nanohybrid: waste to energy insight. Chem. Eng. J. **358** (2019). https://doi.org/10.1016/j.cej.2018.10.096
100. M. Xu et al., Graphene-like two-dimensional materials. Chem. Rev. **113**(5), 3766–3798 (2013). https://doi.org/10.1021/cr300263a
101. Q. Xu et al., S-scheme heterojunction photocatalyst. Chem **6**(7), 1543–1559 (2020). https://doi.org/10.1016/j.chempr.2020.06.010
102. Y. Xu et al., Synthesis of ultrathin CdS nanosheets as efficient visible-light-driven water splitting photocatalysts for hydrogen evolution. Chem. Commun. **49**(84) (2013). https://doi.org/10.1039/c3cc46342g
103. D.A. Yaseen, M. Scholz, Shallow pond systems planted with Lemna minor treating azo dyes. Ecol. Eng. **94** (2016). https://doi.org/10.1016/j.ecoleng.2016.05.081
104. S. Ye et al., Simultaneous removal of organic pollutants and heavy metals in wastewater by photoelectrocatalysis: a review. Chemosphere **273**(xxxx), 128503 (2021). https://doi.org/10.1016/j.chemosphere.2020.128503
105. Z. Yin et al., Au nanoparticle-modified MoS2 nanosheet-based photoelectrochemical cells for water splitting. Small **10**(17), 3537–3543 (2014). https://doi.org/10.1002/smll.201400124
106. J. Yu, X. Yu, Hydrothermal synthesis and photocatalytic activity of zinc oxide hollow spheres. Environ. Sci. Technol. **42**(13) (2008). https://doi.org/10.1021/es800036n
107. X. Yu et al., Ti3C2 MXene nanoparticles modified metal oxide composites for enhanced photoelectrochemical water splitting. Int. J. Hydrogen Energy **44**(5), 2704–2710 (2019). https://doi.org/10.1016/j.ijhydene.2018.11.221
108. C. Zaharia, D. Suteu, *Characteristics, Polluting Effects and Separation/Elimination Procedures from Industrial Effluents – A Critical Overview, Organic Pollutants Ten Years After the Stockholm Convention - Environmental and Analytical*, *Organic Pollutants Ten Years After the Stockholm Convention - Environmental and Analytical Update* (2012)
109. Z. Zeng et al., Single-layer semiconducting nanosheets: High-yield preparation and device fabrication. Angew. Chemie-Int. Edition **50**(47) (2011). https://doi.org/10.1002/anie.201106004
110. Z. Zeng et al., An effective method for the fabrication of few-layer-thick inorganic nanosheets. Angew. Chemie-Int. Edition **51**(36) (2012). https://doi.org/10.1002/anie.201204208
111. G. Zhang, Z. Wang, J. Wu, Construction of a Z-scheme heterojunction for high-efficiency visible-light-driven photocatalytic CO2reduction. Nanoscale **13**(8), 4359–4389 (2021). https://doi.org/10.1039/d0nr08442e
112. W. Zhao et al., Fabrication of a novel p-n heterojunction photocatalyst n-BiVO4@p-MoS2 with core-shell structure and its excellent visible-light photocatalytic reduction and oxidation activities. Appl. Catal. B **185** (2016). https://doi.org/10.1016/j.apcatb.2015.12.023
113. X. Zhao et al., Photoelectrocatalytic oxidation of CuII-EDTA at the TiO 2 electrode and simultaneous recovery of CuII by electrodeposition. Environ. Sci. Technol. **47**(9) (2013). https://doi.org/10.1021/es3046982

114. J. Zheng et al., High yield exfoliation of two-dimensional chalcogenides using sodium naphthalenide. Nat. Commun. **5** (2014). https://doi.org/10.1038/ncomms3995
115. L. Zheng et al., Hierarchical MoS2 nanosheet@TiO2 nanotube array composites with enhanced photocatalytic and photocurrent performances. Small **12**(11) (2016). https://doi.org/10.1002/smll.201503441
116. Z. Zheng, I.M.C. Lo., Fabrication of MoS2@BL-BiVO4 photoanode with promoted charge separation for photoelectrochemical sewage treatment to simultaneously degrade PPCPs, disinfect E. coli, and produce H2: Performance, mechanisms, and influence factors. Appl. Catal. B **299** (2021). https://doi.org/10.1016/j.apcatb.2021.120636
117. C. Zhi et al., Large-scale fabrication of boron nitride nanosheets and their utilization in polymeric composites with improved thermal and mechanical properties. Adv. Mater. **21**(28) (2009). https://doi.org/10.1002/adma.200900323
118. R. Zhu et al., Z scheme system ZnIn2S4/RGO/BiVO4 for hydrogen generation from water splitting and simultaneous degradation of organic pollutants under visible light. Renew. Energy **139**, 22–27 (2019). https://doi.org/10.1016/j.renene.2019.02.049
119. X. Zong et al., Enhancement of photocatalytic H2 evolution on CdS by loading MoS2 as cocatalyst under visible light irradiation. J. Am. Chem. Soc. **130**(23) (2008). https://doi.org/10.1021/ja8007825
120. X. Zong et al., Photocatalytic H2 evolution on MoS2/CdS catalysts under visible light irradiation. J. Phys. Chem. C 114(4) (2010). https://doi.org/10.1021/jp904350e
121. X. Zong et al. Photocatalytic H2 evolution on CdS loaded with WS2 as cocatalyst under visible light irradiation. J. Phys. Chem. C 115(24) (2011). https://doi.org/10.1021/jp2006777